

超快激光旋光钻孔孔径和锥度的控制

阿占文^{1,2*}, 陈灵灵¹, 吴影¹, 杜荣葆¹, 白海林¹, 邹贵生¹¹清华大学机械工程系, 北京 100084;²青海大学机械工程学院, 青海 西宁 810016

摘要 孔径和锥度的控制是超快激光微孔加工面临的难点之一, 旋光钻孔是控制孔径和锥度的有效手段。因此, 针对道威棱镜旋光钻孔系统, 首先, 从几何光学的角度研究了聚焦后激光出射角度和光斑旋转直径与可平移反射镜位置、楔形棱镜旋转角之间的关系。然后, 利用 CCD 相机分别测量实际光斑在焦平面、焦平面上下 $\pm 250 \mu\text{m}$ 处的旋转直径, 并在厚度为 0.5 mm 的黄铜板上进行钻孔实验, 得到深径比为 6:1、锥度为 $-2.6^\circ \sim 2.3^\circ$ 的微孔。对比实验得到的微孔出入口直径与 CCD 相机的测量结果, 得到孔径、锥度与光束旋转角之间的关系。结果表明, 孔径主要由楔形棱镜旋转角决定, 调整可平移反射镜的位置可得到不同锥度的微孔; 激光能量的变化会影响材料的去除, 因此, 焦点位置、激光平均功率以及光斑重叠率也会在小范围内影响孔径和锥度。

关键词 激光技术; 超快光学; 旋光微孔加工; 道威棱镜; 孔径; 锥度

中图分类号 O439

文献标志码 A

doi: 10.3788/CJL202148.0802017

1 引言

直径为数十到数百微米的微孔及微孔阵列广泛应用于航空、汽车制造等行业, 这些行业对微孔加工精度和材料的要求较高, 而放电加工、电化学加工^[1]等传统微细加工手段多受效率、材料选择性和精度的限制。超快激光(脉宽小于 10 ps)的峰值功率极高, 可加工高温合金^[2-4]、宝石^[5-7]、陶瓷^[8-9]、玻璃^[10-15]等硬脆、难加工的材料, 同时又具有非接触加工和效率高的优势。孔径和锥度的控制是超快激光微孔加工面临的重点难题之一, 目前五轴扫描振镜可实现孔径和锥度的控制^[16], 但该设备价格昂贵, 且加工工艺复杂。超快激光旋光钻孔系统具有孔径和锥度可调且孔形不受光斑形状和偏振状态影响等优势, 是微孔加工与应用的研究热点。

基于道威棱镜(Dove prism)的旋光钻孔系统, 锥度和孔径的控制主要受可平移反射镜位置和楔形棱镜旋转角的影响, 目前对不同参数相互之间的关系仅有定性描述而无系统研究。关于超快激光多脉

冲叩击钻孔、环形钻孔的直径和锥度控制研究主要从激光本身(单脉冲能量、频率等)及加工参数(辅助方式、材料)的角度开展^[17], 且其与旋光钻孔的原理不同, 无法应用于旋光钻孔系统。因此, 本文在研究道威棱镜旋光钻孔光路的基础上, 通过实验研究了其锥度和孔径的控制机理。此外, 改变光束角度和旋转直径的控制参数后, 本方法也可用于多光楔、三级反射镜等不同旋光系统中锥度、孔径的控制。

2 道威棱镜旋光钻孔光路

道威棱镜旋光钻孔系统由反射镜(M1)、半波片(HWP0)、可平移反射镜(M2)、楔形棱镜(WP0)、旋转光学、平衡光学、聚焦及视觉部分组成。其中, 旋转光学部分由半波片(HWP1)、道威棱镜组成; 平衡光学由平板镜(PP)和一对楔形棱镜组(WP1、WP2)构成; 聚焦及视觉部分安装在可上下移动的精密运动平台上, 由同轴的 CCD 相机、吹气装置和聚焦镜组成。此外, 可平移反射镜、楔形棱镜、旋转光学、XYZ 三轴精密运动平台均由计算机控制,

收稿日期: 2020-12-01; 修回日期: 2021-01-04; 录用日期: 2021-02-23

基金项目: 国家重点研发计划(2017YFB1104900)、国家自然科学基金(51775299, 52075287)、国家自然科学基金国际(地区)合作与交流项目(51520105007)

* E-mail: azw19@mails.tsinghua.edu.cn

运动平台可精确控制工件的位移,同时输出触发激光器的脉冲信号,如图 1 所示。通过移动反射镜 M2 可改变聚焦前激光束的入射位置,从而获得

不同的出射光束角度;旋转楔形棱镜 WP0 可改变聚焦前激光束的入射角度,从而获得不同的旋转直径。

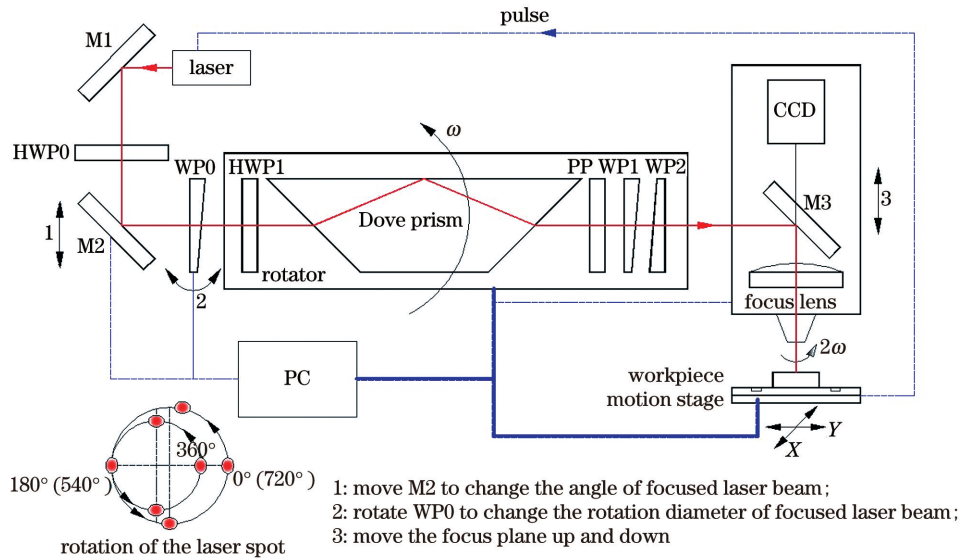


图 1 基于道威棱镜的旋光钻孔系统

Fig. 1 Optical rotation drilling system based on the Dove prism

微孔加工实验在厚度为 0.5 mm 的黄铜板上进行,激光的脉冲宽度为 1 ps,波长为 515 nm,单脉冲能量固定为 87 μJ ,脉冲频率在 50~100 kHz 范围内可调,焦点位置位于黄铜板厚度(板厚)的中心。用压强为 250 kPa 的压缩空气作为辅助气体通过同轴吹气的方式由上而下吹向铜板上表面。光束转速为 4000 r/min,钻孔时间均为 11 s。分别调整楔形棱镜的旋转角和可平移反射镜的位置,利用 CCD 相机分别测量实际光斑在焦平面以及焦平面上下 $\pm 250 \mu\text{m}$ 处的旋转直径。由于焦点在板厚中心,因此焦平面上下 $\pm 250 \mu\text{m}$ 处的光斑旋转即微孔入口、出口处的光斑旋转。

旋光钻孔最大的优势在于钻孔直径和锥度可控,此外,高速旋转的光斑可减少光束偏振和光斑形状(非标准圆形)造成的影响。旋转光学和平衡光学由空心轴电机带动一起高速旋转(转速最高为 5000 r/min);当道威棱镜的旋转角速度为 ω 时,穿过道威棱镜激光光束的旋转角速度为 2ω (转速最高为 10000 r/min)。高速旋转的光斑使激光能量分布更均匀,从而减小光斑形状对系统的影响。激光器输出的激光为线性偏振,利用振镜进行扫描钻孔时,光斑的偏振方向保持不变,导致孔的某一对称位置为 s 偏振,相隔 90° 处为 p 偏振。当钻孔进行到一定阶段时孔壁出现一定角度的倾斜,此时孔壁对 s 偏振光和 p 偏振光的反射率不同,导致孔在垂直于偏

振方向的直径增大,孔出口的圆度变差^[17-21],可将线偏振光转换为圆偏振光或借助旋转光学设备使线偏振光随光斑高速旋转解决该问题。道威棱镜的制造及安装误差使实际的光斑轨迹不是理想的同心圆,即光斑轨迹转过第一圈后起点、终点并不重合(如图 1 中的左下角部分),导致光束聚焦后的出射角度发生变化;此外,旋转直径的变化导致光斑在不同位置具有不同的旋转线速度,从而影响光斑的重叠率,造成能量密度不均匀分布。改变平衡光学中平板镜的角度可小幅度偏转出射光束,使旋转的光斑在 0° 时向直径变小的方向移动,在 360° 时向直径变大的方向移动,从而补偿该误差。

3 孔径和锥度的控制

3.1 影响孔径与锥度的因素

在旋光钻孔中,孔径主要由光斑的旋转直径决定,且受单个光斑对材料去除区域大小的影响。对于同一材料,激光经过聚焦透镜后单个光斑的去除区域大小取决于离焦量和平均功率。由于实际加工中无法精确定位光束焦点的位置,因此需要研究离焦量对孔径的影响。假设激光波长 $\lambda = 515 \text{ nm}$,光束质量 $M^2 = 1.1$,焦距 $f = 60 \text{ mm}$,聚焦前入射光束的直径 $D = 3 \text{ mm}$,计算得到激光相对光强 I/I_0 (I_0 为焦点处光斑中心的光强, I 为不同光斑半径处的光强)的高斯分布曲线随离焦量的变化如图 2(a)所

示,其中 r 为光斑半径。可以发现,对于光强分布截面,焦点处的光强分布曲线被收紧,而离焦后曲线被展宽。除离焦量外,激光的平均功率也会影响材料去除的范围,在相同参数下改变激光的平均功率,得到激光相对光强的高斯分布曲线如图 2(b) 所示。可以发现,当激光功率增大时,相同光强对应的光斑

半径增大。此外,脉冲激光钻孔中光斑重叠率也会影响孔的直径,光斑重叠率为单位面积的激光能量,由光斑大小、脉冲频率、旋转直径($2R$)和旋转速度共同决定,旋光钻孔的光斑重叠率和不同旋转直径 d 下脉冲频率与光斑重叠率的关系如图 2(c)、图 2(d) 所示。

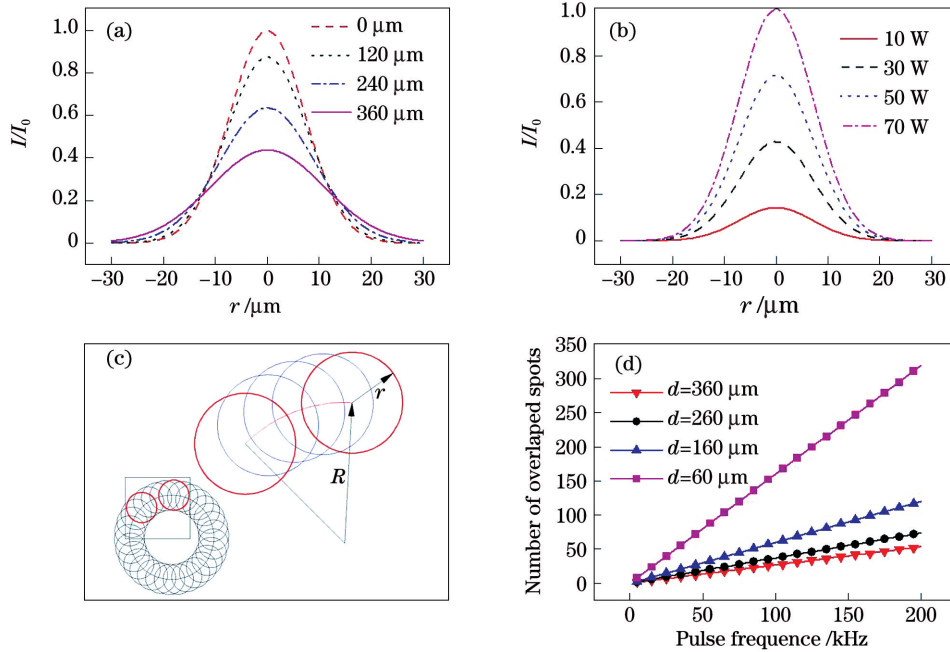


图 2 离焦量、激光平均功率和光斑重叠率对孔径的影响。(a)光强随离焦量的变化曲线;(b)光强随平均功率的变化曲线;(c)旋光钻孔光斑的重叠率;(d)不同旋转直径下脉冲频率与光斑重叠率的关系

Fig. 2 Effect of defocusing amount, laser average power and spot overlap rate on aperture. (a) Change curve of the light intensity with defocusing amount; (b) change curve of the light intensity with average power; (c) overlap rate of the optical rotation drilling spot; (d) relationship between pulse frequency and spot overlap rate under different rotation diameters

为了从几何光学角度研究光斑中心的旋转直径和聚焦激光束倾斜角与光路参数的关系,假设入射光线为 AB ,斜率为 k ,如图 3(a) 所示。利用副光轴法可求得出射光线与焦平面交点 C (副焦点)的坐标为 (f, kf) ,焦平面上光斑中心的旋转直径为

$$d = 2|\overrightarrow{CF}| = 2k \cdot f = 2f \cdot \tan \varphi, \quad (1)$$

式中, φ 为入射光线与主光轴的夹角,如图 3(b) 所示。可以发现,焦平面上光斑中心的旋转直径取决于聚焦前光束与光轴的夹角,而光路中只有楔形棱镜旋转角会影响聚焦前的光束角度。

光束聚焦后的倾斜角 β 可表示为

$$\tan \beta = \left| \tan \varphi - \frac{a}{f} \right|, \quad (2)$$

式中, a 为光束与聚焦透镜中心的偏移量。可以发现,聚焦前入射光束的入射角 φ 和光束偏移量 a 共同决定了聚焦激光束的倾斜角。

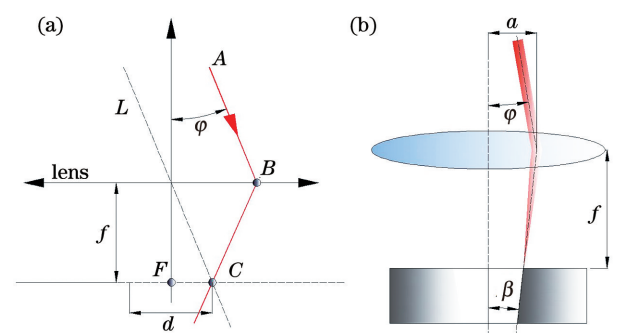


图 3 调整孔径和锥度的原理图。(a)求解孔径和锥度的原理图;(b)孔径和锥度的示意图

Fig. 3 Schematic diagram of the adjusting aperture and taper. (a) Schematic diagram of the solving aperture and taper; (b) schematic diagram of the aperture and taper

3.2 孔径的控制

光束通过楔形棱镜时经历 2 次折射,随着楔形

棱镜旋转角的增加,会出现 2 种光路,如图 4 所示。其中, α 为楔形棱镜楔角, θ 为楔形棱镜旋转角, η 为

光束发生第 1 次折射时的出射角, γ 为光束发生第 2 次折射时的出射角, i 为楔形棱镜的折射率。

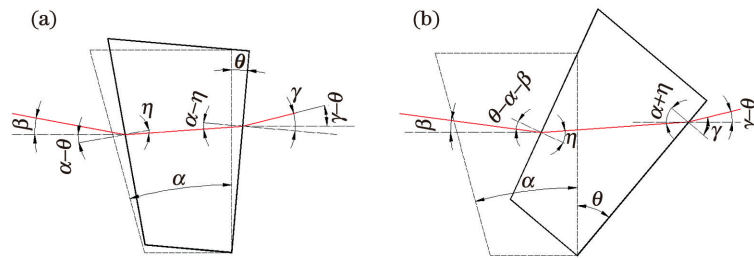


图 4 楔形棱镜旋转角与光束出射角的关系。(a) $\theta \leq \alpha + \beta$; (b) $\theta > \alpha + \beta$

Fig. 4 Relationship between the angle of the wedge prism and the angle of emergence. (a) $\theta \leq \alpha + \beta$; (b) $\theta > \alpha + \beta$

光线发生第一次折射时的入射角为 $\alpha + \beta - \theta$, 出射角为 η ; 光束发生第 2 次折射时的入射角为 $\alpha -$

η , 出射角为 γ , 通过楔形棱镜的出射光束与光轴的夹角为 $\gamma - \theta$ 。由折射定律可知, 当 $\theta \leq \alpha + \beta$ 时

$$\varphi = \gamma - \theta = \arcsin [i \cdot \sin(\alpha - \eta)] - \theta = \arcsin \left\{ i \cdot \sin \left[\alpha - \arcsin \left[\frac{\sin(\beta + \alpha - \theta)}{i} \right] \right] \right\} - \theta. \quad (3)$$

当楔形棱镜旋转角 $\theta > \alpha + \beta$ 时, 同理可得

$$\varphi = \gamma - \theta = \arcsin [i \cdot \sin(\alpha + \eta)] - \theta = \arcsin \left\{ i \cdot \sin \left[\alpha + \arcsin \left[\frac{\sin(\theta - \alpha - \beta)}{i} \right] \right] \right\} - \theta. \quad (4)$$

由于正弦和反正弦函数均为奇函数, 因此(3)式和(4)式等价, 结合(1)式, 可得到光斑旋转中心直径与楔形棱镜旋转角 θ 的定量关系。利用 CCD 相机在焦平面上测量聚焦后激光光斑中心的旋转直径并与用公式计算的结果进行对比, 结果如图 5 所示。可以发现, 焦平面上光斑的旋转直径由楔形棱镜旋转角决定, 实测的结果与理论计算结果相吻合。

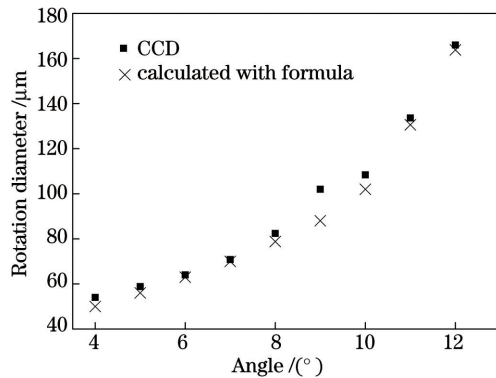


图 5 焦平面上光斑旋转直径与楔形棱镜旋转角的关系
Fig. 5 Relationship between the rotation diameter of the spot and the angle of the wedge prism on the focal plane

3.3 锥度的控制

调整可平移反射镜的位置可以改变聚焦光束的出射角, 从而改变微孔的锥度, 但出射角并不等于锥度, 二者之间的关系还需通过实验进行分析。当楔形棱镜旋转角在 $5^\circ \sim 10^\circ$ 范围内可调, 可平移反射镜

的位置由 -4 mm 移动到 3 mm 时, 用 CCD 分别测量焦平面及焦平面上下 $\pm 250 \text{ }\mu\text{m}$ 处的光斑旋转直径。实验中激光焦点位于板厚中心, 铜板厚度为 0.5 mm , 因此, 在不考虑扰动的情况下, 焦平面及焦平面上下 $\pm 250 \text{ }\mu\text{m}$ 处的光斑旋转分别代表孔纵向中心、入口、出口的光斑旋转情况。将 CCD 测得的光斑中心旋转直径与相同参数下实际加工出的微孔出入口直径进行对比, 得出锥度的变化规律。当楔形棱镜旋转角为 10° 时, CCD 相机的测量结果与实际钻孔结果如图 6(a) 所示。可以发现, 当可平移反射镜的位置由 -4 mm 移动到 3 mm 时, 焦平面上方 $250 \text{ }\mu\text{m}$ 处的光束旋转直径由小变大, 焦平面上的光束旋转直径基本保持恒定, 焦平面下方 $250 \text{ }\mu\text{m}$ 处的光束旋转直径则由大变小。CCD 相机测量的聚焦光束出射角如图 6(b) 所示, 可以发现, 出射角以焦点为中心发生变化, 这表明调整可平移反射镜的位置可改变聚焦光束的出射角, 进而控制锥度。聚焦光束的出射角并不代表实际的锥度, 在楔形棱镜旋转角固定时, 孔出口直径与焦平面上光斑旋转直径的变化规律类似, 二者的差值基本恒定, 且改变可平移反射镜位置时, 两者的变化都比较小。与孔出口直径不同, 孔入口直径随着焦平面上方 $250 \text{ }\mu\text{m}$ 处光束旋转直径的增大而增大, 微孔出入口直径的变化如图 6(c) 所示。可以发现, 出口直径不变, 入口直径的变化会导致锥度的变化。基于该原理, 实

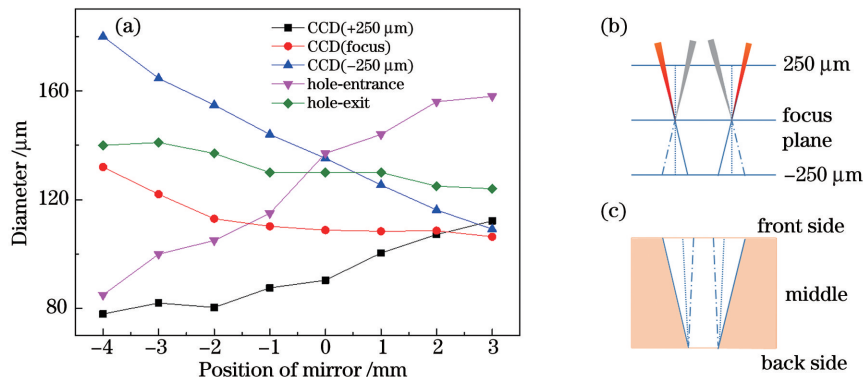


图 6 光斑旋转直径和孔出入口直径的关系。(a)光斑旋转直径和孔出入口直径、可平移反射镜位置的变化曲线;(b)聚焦光束的出射角度;(c)微孔锥度

Fig. 6 Relationship between the spot rotation diameter and the diameter of the entrance and exit of the hole. (a) Change curves of the spot rotation diameter, the diameter of the entrance and exit of the hole, and the position of the translational mirror; (b) exit angle of the focused beam; (c) taper of the micro-hole

验加工出锥度可在 $-2.6^{\circ} \sim 2.3^{\circ}$ 范围内变化的微孔,其中,负锥度表示微孔入口小于出口的情况。

当距离焦平面 $\pm 250 \mu\text{m}$ 处的光斑旋转直径比为 0.66 时,孔锥度接近 0° ,比值更小时可得到负锥度。当比值为 1 时,虽然光斑旋转直径相等,但实际

加工出的微孔仍存在正锥度,变化情况如表 1 所示。此外,在微孔加工时,无论旋转直径如何变化,孔出口直径变化均很小,原因是激光在微孔内传输时能量会逐渐衰减。为得到零锥度的直孔,入口处光斑的旋转直径要小于出口处的旋转直径。

表 1 锥度与激光光斑旋转直径的关系

Table 1 Relationship between taper and the rotation diameter of the laser spot

Mirror position / mm	-3	0	3	4
	$d = 80 \mu\text{m}$ (+250 μm)	$d = 90 \mu\text{m}$ (+250 μm)	$d = 112 \mu\text{m}$ (+250 μm)	$d = 121 \mu\text{m}$ (+250 μm)
Rotation of spot (measured by CCD)				
	$d = 154 \mu\text{m}$ (-250 μm)	$d = 136 \mu\text{m}$ (-250 μm)	$d = 110 \mu\text{m}$ (-250 μm)	$d = 102 \mu\text{m}$ (-250 μm)
	entrance exit	entrance exit	entrance exit	entrance exit
	$d = 135 \mu\text{m}$ $d = 167 \mu\text{m}$	$d = 167 \mu\text{m}$ $d = 162 \mu\text{m}$	$d = 188 \mu\text{m}$ $d = 154 \mu\text{m}$	$d = 197 \mu\text{m}$ $d = 150 \mu\text{m}$
Hole size				
Taper				
	taper less than 0	taper equal 0	tape more than 0	taper more than 0

微孔加工时脉冲频率、单脉冲能量以及焦点位置会影响加工效率和孔形。如果焦点位于材料上表面,相同时间内(实验中加工时间为 11 s)微孔甚至

无法被完全贯穿。因此,为了加工更大的微孔,需提高脉冲频率以保持恒定的能量输入。否则,加工效率和孔形均会变得不理想。

直径为 $100\ \mu\text{m}$ 的微孔截面在扫描电子显微镜下的观察结果如图 7(a)、图 7(b) 所示,其锥度约为 0.6° 。可以发现,在整个孔深范围内,直径一致度较好;除入口处侧壁有纵向条纹外,其余各处侧壁均比较光滑。在部分情况下,孔出入口的质量较好,但部分微孔出入口的质量存在一定瑕疵。从图 7(c) 中可以发现,同一参数下多次实验得到的微孔具有很高的重复性,且缺陷的位置和形貌也具有重复性。图 7(d) 为入口边缘有损伤及残渣堆积的情况,图 7(e) 是一种出口接近椭圆,且背部有损伤的情况,原因可能是道威棱镜对光束偏振有一定的扰动^[22],无法得到理想的旋转线性偏振,在特定角度下材料对 p 偏振和 s 偏振的反射率不同。为了不破坏样品的原始形貌,样品未经任何化学处理。

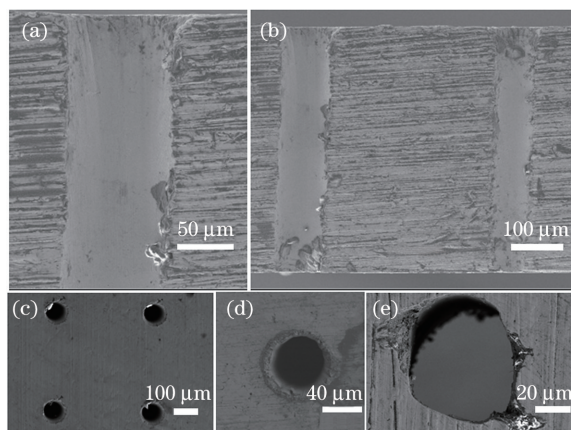


图 7 微孔截面及出入口的形貌。(a)~(b)微孔截面;
(c)~(d)微孔入口;(e)微孔出口

Fig. 7 Morphology of the cross section, entrance and exit of the micropore. (a)–(b) Micropore cross section; (c)–(d) micropore entrance; (e) micropore exit

4 结 论

针对道威棱镜旋光钻孔系统,研究了孔径与锥度的控制原理。利用 CCD 相机分别测量了实际光斑在焦平面、焦平面上下 $\pm 250\ \mu\text{m}$ 处的旋转直径。将焦点定位在板厚中心,在厚度为 $0.5\ \text{mm}$ 的黄铜板上进行钻孔实验,加工出了深径比为 $6:1$,锥度为 $-2.6^\circ \sim 2.3^\circ$ 的微孔。将实验得到的微孔出入口直径与 CCD 相机的测量结果进行对比,得到孔径、锥度与光束旋转角度之间的关系如下。

1) 孔径主要由楔形棱镜的旋转角决定。确定孔径后,调整可平移反射镜位置可得到不同锥度的微孔。激光能量的变化会影响材料的去除,因此焦点位置、激光平均功率以及光斑重叠率间接在小范

围内会影响孔径和锥度。

2) 移动可平移反射镜的位置可以改变聚焦光束的出射角,进而控制锥度。但聚焦光束的出射角并不是实际的锥度,还需考虑孔内的激光能量衰减。当楔形棱镜旋转角固定,改变可平移反射镜的位置时,孔出口直径变化很小,但孔入口直径有明显变化,从而得到负锥度、零锥度(直孔)和正锥度的微孔。

3) 实验发现部分情况下微孔出入口表面质量和圆度存在一定缺陷,且同一参数下多次实验得到的微孔缺陷位置和形貌具有很高的重复性,需进一步研究其产生及消除机理。此外,孔内激光能量的传输过程是锥度控制中的重要因素,而实验以固定的钻孔时间研究了孔径和锥度的控制,未研究孔在深度方向上随时间演变的规律。

参 考 文 献

- [1] Rahman Z, Das A K, Chattopadhyaya S. Microhole drilling through electrochemical processes: a review [J]. *Materials and Manufacturing Processes*, 2018, 33(13): 1379-1405.
- [2] Zheng C L, Zhao K, Shen H, et al. Crack behavior in ultrafast laser drilling of thermal barrier coated nickel superalloy [J]. *Journal of Materials Processing Technology*, 2020, 282: 116678.
- [3] Li Q, Yang L J, Hou C J, et al. Surface ablation properties and morphology evolution of K24 nickel based superalloy with femtosecond laser percussion drilling [J]. *Optics and Lasers in Engineering*, 2019, 114: 22-30.
- [4] Liu H D, Zhao W Q, Wang L Z, et al. Percussion drilling of deep holes using picosecond ultrashort pulse laser in Ni-based superalloy coated with ceramic thermal barrier coatings [J]. *Materials*, 2020, 13 (16): 3570.
- [5] He C, Zibner F, Fornaroli C, et al. High-precision helical cutting using ultra-short laser pulses [J]. *Physics Procedia*, 2014, 56: 1066-1072.
- [6] Li Z Q, Wu Q, Wang J. Ultrashort pulsed laser micromachining of polycrystalline diamond [J]. *Advanced Materials Research*, 2012, 497: 220-224.
- [7] Jeong B, Lee B, Kim J H, et al. Drilling of sub- $100\ \mu\text{m}$ hourglass-shaped holes in diamond with femtosecond laser pulses [J]. *Quantum Electronics*, 2020, 50(2): 201-204.
- [8] Narazaki A, Takada H, Yoshitomi D, et al. Study on nonthermal-thermal processing boundary in

- drilling of ceramics using ultrashort pulse laser system with variable parameters over a wide range [J]. *Applied Physics A*, 2020, 126(4): 1-8.
- [9] Wang Y Q, Zhang J Z, Liu Y S, et al. Effect of femtosecond laser parameters on TiC ceramic micro-hole drilling[J]. *Chinese Journal of Lasers*, 2014, 41(10): 1003010.
王禹茜, 张军战, 刘永胜, 等. 飞秒激光工艺参数对加工 TiC 陶瓷微孔的影响 [J]. *中国激光*, 2014, 41(10): 1003010.
- [10] Xing S L, Liu L, Zou G S, et al. Effects of femtosecond laser parameters on hole drilling of silica glass[J]. *Chinese Journal of Lasers*, 2015, 42(4): 0403001.
邢松龄, 刘磊, 邹贵生, 等. 飞秒激光参数对石英玻璃微孔加工的影响 [J]. *中国激光*, 2015, 42(4): 0403001.
- [11] Lee H M, Choi J H, Moon S J. Determining the machining parameters for femtosecond laser helical drilling of aluminosilicate glass substrate [J]. *International Journal of Precision Engineering and Manufacturing*, 2017, 18(7): 923-930.
- [12] Karimelahi S, Abolghasemi L, Herman P R. Rapid micromachining of high aspect ratio holes in fused silica glass by high repetition rate picosecond laser [J]. *Applied Physics A*, 2014, 114(1): 91-111.
- [13] Jiang L, Liu P J, Yan X L, et al. High-throughput rear-surface drilling of microchannels in glass based on electron dynamics control using femtosecond pulse trains[J]. *Optics Letters*, 2012, 37(14): 2781-2783.
- [14] Wlodarczyk K L, Brunton A, Rumsby P, et al. Picosecond laser cutting and drilling of thin flex glass [J]. *Optics and Lasers in Engineering*, 2016, 78: 64-74.
- [15] Ito Y, Shinomoto R, Nagato K, et al. Mechanisms of damage formation in glass in the process of femtosecond laser drilling [J]. *Applied Physics A*, 2018, 124(2): 1-8.
- [16] Auerswald J, Ruckli T, Weber P, et al. Taper angle correction in cutting of complex micro-mechanical contours with ultra-short pulse laser [J]. *Journal of Mechanics Engineering and Automation*, 2016(7): 334-338.
- [17] Nath A K. Laser drilling of metallic and nonmetallic substrates[J]. *Comprehensive Materials Processing*, 2014, 9: 115-175.
- [18] Gaudfrin K, Lopez J, Mishchik K, et al. Fused silica ablation by double femtosecond laser pulses: influence of polarization state [J]. *Optics Express*, 2020, 28(10): 15189-15206.
- [19] Nolte S, Momma C, Kamlage G, et al. Polarization effects in ultrashort-pulse laser drilling [J]. *Applied Physics A*, 1999, 68(5): 563-567.
- [20] Wang R J, Dong X, Wang K D, et al. Polarization effect on hole evolution and periodic microstructures in femtosecond laser drilling of thermal barrier coated superalloys[J]. *Applied Surface Science*, 2021, 537: 148001.
- [21] Cho J H, Na S J. Theoretical analysis of keyhole dynamics in polarized laser drilling [J]. *Journal of Physics D: Applied Physics*, 2007, 40(24): 7638-7647.
- [22] Moreno I, Paez G, Strojnik M. Polarization transforming properties of Dove prisms [J]. *Optics Communications*, 2003, 220(4/5/6): 257-268.

Controlling of Diameter and Taper in Ultrafast Laser Helical Drilling

A Zhanwen^{1,2*}, Chen Lingling¹, Wu Ying¹, Du Rongbao¹, Bai Hailin¹, Zou Guisheng¹

¹Department of Mechanical Engineering, Tsinghua University, Beijing 100084, China;

²School of Mechanical Engineering, Qinghai University, Xining, Qinghai 810016, China

Abstract

Objective Taper-free or negative conical micro-holes with a diameter of tens to few hundreds of microns are of great interest in a variety of industries. Conventional methods, such as electro-discharge drilling, mechanical drilling, electrochemical drilling, and continuous or pulsed laser drilling, have their limitations, including poor accuracy, low efficiency, as well as they are incapable of drilling in non-conductive materials, such as glass. Although ultrafast laser is believed to be a reliable tool for drilling processes due to its unique characteristics, the control of the diameter and taper of micro-holes is one of the greatest challenges encountered in the process. At present, the diameter and taper of micro-holes can be controlled using a 5-axis Galvano scanner, but the equipment is expensive, and a complex drilling strategy is required. Ultrafast laser helical drilling technology is an effective and

simple way to adjust the taper and diameter of micro-holes since the laser spot is rotated at a high speed, and the roundness of the holes can be improved in the meantime. However, the taper and diameter are affected by several factors in helical drilling, and these factors vary with material, aspect ratio, laser characteristics, and drilling strategy. Hence, it is important and necessary to investigate the relationship between the diameter, taper, and beam rotation of micro-holes and to show the control mechanism of the diameter and taper in ultrafast laser helical drilling.

Methods With the ultrafast laser focused in the middle of a 0.5 mm thick copper plate, various micro-holes with different diameters and taper are drilled by adjusting the angle of the focused beam and rotation diameter of the laser spot. Then the rotation diameter of the laser spot at a focal plane, $\pm 250 \mu\text{m}$ above and below the focal plane, is in situ monitored by a CCD. The diameters of the micro-holes in the entrance and exit are compared with the CCD measurement results at $\pm 250 \mu\text{m}$ above and below the focal plane, respectively. The dependence of the spot rotation diameter on the angle of the wedge prism is analyzed based on geometric optics.

Results and Discussions Micro-holes with an aspect ratio of 6 : 1 and taper of $-2.6^\circ - 2.3^\circ$ are obtained, and the relationship between the micro-hole diameter, taper, and beam rotation characteristics is shown (**Table 1**). The rotation diameter of the spot measured by the CCD and the diameter of the micro-hole drilled under the same parameters are investigated (**Fig. 6(a)**). When the position of the movable mirror changes from -4 mm to 3 mm , the diameter of the rotation beam changes from a small value to a large value at $250 \mu\text{m}$ above the focal plane and from a large value to a small value at $250 \mu\text{m}$ below the focal plane, while the diameter remains constant at the focal plane. This means that the focused beam rotates around the focus point (**Fig. 6(b)**). However, the angle of the focused beam does not equal the actual taper. Under a fixed wedge prism angle, the change in the hole diameter on the exit side is similar to that of the spot rotation diameter on the focal plane, the changes vary slightly, and the difference between them is almost constant. In contrast, the diameter of the hole entrance increases with the beam rotation diameter at $250 \mu\text{m}$ above the focal plane. That is, the hole diameter of the exit side remains unchanged, and the diameter change of the entrance side will lead to the change of the taper (**Fig. 6(c)**). It is based on this principle that micro-holes with a taper varying from -2.6° to 2.3° are machined in which a negative taper represents that the entrance of the micro-hole is smaller than the exit. Besides, when the rotation diameter ratio of the spot at $\pm 250 \mu\text{m}$ from the focal plane is 0.66, the hole taper is close to 0° , and a negative taper can be obtained when the ratio is smaller. When the ratio is 1, although the spot rotation diameter is constant, there is still a positive taper in the micro-hole. The diameter of the exit changes marginally no matter how much the rotation diameter changes because the laser energy is attenuated during the transmission in the micro-hole. The rotation diameter of the spot at the entrance must be smaller than that at the exit to get a straight hole with zero tapers. The pulse energy, frequency, and focus position will affect the processing efficiency and the shape of the hole. If the laser is focused on the surface of the workpiece, the micro-holes cannot penetrate completely under the same drilling time.

Conclusions In this study, we showed the relationship between the micro-hole diameter, taper, and beam rotation in a Dove-prism-based helical drilling system. The results show that the micro-hole size is dominated by the angle of the wedge prism. As for the taper of the micro-hole, adjusting the position of the movable mirror can change the exit angle of the focused beam, and then the taper can be adjusted. Since the laser energy will affect the ablation rate of material, the focus position, laser power, and spot overlap rate will slightly contribute to the micro-hole size and taper.

Key words laser technique; ultrafast laser; micro-hole helical drilling; Dove prism; diameter; taper

OCIS codes 320.7090; 140.3390; 160.2750